

Measuring the Top Yukawa Coupling at 100 TeV

Michelangelo L. Mangano

CERN, PH-TH, 1211 Geneva 23, Switzerland

E-mail: michelangelo.mangano@cern.ch

Tilman Plehn

Institut für Theoretische Physik, Universität Heidelberg, Germany

E-mail: plehn@uni-heidelberg.de

Peter Reimitz

Institut für Theoretische Physik, Universität Heidelberg, Germany

E-mail: p.reimitz@thphys.uni-heidelberg.de

Torben Schell

Institut für Theoretische Physik, Universität Heidelberg, Germany

E-mail: schell@thphys.uni-heidelberg.de

Hua-Sheng Shao

CERN, PH-TH, 1211 Geneva 23, Switzerland

E-mail: huasheng.shao@cern.ch

Abstract. We propose a measurement of the top Yukawa coupling at a 100 TeV hadron collider, based on boosted Higgs and top decays. We find that the top Yukawa coupling can be measured to 1%, with excellent handles for reducing systematic and theoretical uncertainties, both from side bands and from $t\bar{t}H/t\bar{t}Z$ ratios.

Submitted to: *J. Phys. G: Nucl. Phys.*

Contents

1	Introduction	2
2	Theoretical systematics for the $t\bar{t}H/t\bar{t}Z$ production rate	3
2.1	Total rates and ratios	4
2.2	Kinematical distributions	7
3	Boosted $t\bar{t}H$ at 100 TeV	8
4	Updated BDRS tagger	10
5	Outlook	12

1. Introduction

After the discovery of a light and likely fundamental Higgs boson during the LHC Run I [1, 2], the test of the Standard Model nature of this Higgs boson will be one of the key goals of the upcoming LHC run(s). One of the most interesting parameters of the Standard Model (SM) is the top Yukawa coupling y_t . One reason is that, because of its large size, it dominates the renormalization group evolution of the Higgs potential to higher, more fundamental energy scales [3]. On the other hand, this coupling is one of the hardest to directly determine at colliders [4, 5], because this requires a precise measurement of the $t\bar{t}H$ production cross section. This cross section can in principle be measured at hadron colliders [6, 7, 8] as well as at e^+e^- colliders [9, 10]. However, a suitable e^+e^- collider should at least have an energy of 500 GeV. If a future e^+e^- Higgs factory should have lower energy, the precise measurement of y_t will have to be postponed to a future hadron collider, such as the 100 TeV pp collider under consideration at CERN [11] and in China [12].

The global set of physics opportunities of such a 100 TeV collider is being explored in many studies. Obvious pillars of the physics program will include the study of weakly interacting thermal dark matter [14], the gauge sector at high energies [15], the complete understanding of the nature of the electroweak phase transition [16], and shedding more light on the hierarchy problem. The picture will rapidly evolve in the near future, also in view of the forthcoming results for the search of new physics at the LHC, in the experiments dedicated to the study of flavor and CP violating phenomena, and at the astro/cosmo frontier. Nevertheless, the continued study of Higgs properties, pushing further the precision of LHC measurements, exploring rare and forbidden decays, and unveiling the whole structure of the electroweak symmetry-breaking sector [17], will provide the underlying framework for the whole program.

These goals and benchmarks are, already today, clearly defined, allowing us to start assessing their feasibility. For example, first studies indicate that a SM Higgs self-coupling could be measured at 100 TeV with a precision of 5-10% [18], for an integrated luminosity of 30 ab^{-1} , consistent with the current expectations [19]. Similar 100 TeV studies, for the Higgs couplings that are already under investigation at the LHC, are still missing. The fact that already at the high-luminosity LHC (HL-LHC) the couplings' extraction will be dominated by systematic and theoretical uncertainties [20], makes it hard to produce today reliable predictions. One important exception, where statistics may still be limited at the HL-LHC, is $t\bar{t}H$ production. This measurement is also a key ingredient for the determination of the Higgs self-coupling.

In this paper we will show that a precision measurement of the top Yukawa coupling y_t should be added to the main physics opportunities of a 100 TeV hadron collider. The crucial distinction between this measurement at 100 TeV w.r.t. LHC energies is the potential to fully exploit the features of boosted objects and jet substructure [21], thanks to a large-statistics sample of highly boosted top and Higgs particles, as shown in Fig. 1. Our analysis will be based on the first HEPTOPTAGGER

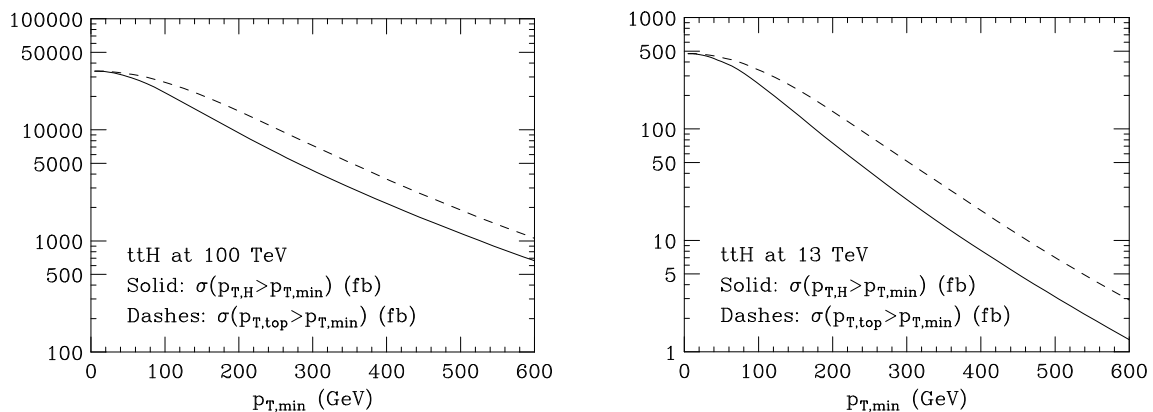


Figure 1: Integrated transverse momentum distributions for the Higgs boson and top (anti-top) quark, in the $t\bar{t}H$ process at a 100 TeV collider (left) and the 13 TeV LHC (right).

application to $t\bar{t}H$ production with a Higgs decay to bottoms [6]. There are three differences between the original LHC analysis [6] and this 100 TeV analysis:

First, the statistically limited LHC analysis of boosted $t\bar{t}H$ production will benefit from the hugely increased statistics with a 100 TeV collider energy and an integrated luminosity of few tens of ab^{-1} . For example, Fig. 1 shows that requesting $p_{T,H} > 500$ GeV gives a rate of $\mathcal{O}(1)$ pb, or 10M events with 10 ab^{-1} . This improved statistics also allows us to rely on a well-measured and similarly peaked $t\bar{t}Z \rightarrow t\bar{t}b\bar{b}$ signal to reduce systematic and theoretical uncertainties. In particular, we will show in Section 2 that the cross section ratio $\sigma(t\bar{t}H)/\sigma(t\bar{t}Z)$ is subject to very small theoretical uncertainties, which, already today, are in the range of a percent. This precision will certainly improve with future calculations.

Second, in Fig. 1 we see that the typical transverse momentum spectra of all particles are significantly harder, giving us a larger relative fraction of events with $p_{T,t} > m_t$ and $p_{T,H} > m_H$. The corresponding results with default taggers will be shown in Section 3.

Finally, the recent improvement in the HEPTOPTAGGER2 [22] and in the BDRS Higgs tagger [23] will allow us to avoid background sculpting and to increase the signal statistics. This last set of improvements will be applied in Section 4. We will find that the ratio between fiducial cross sections for the $t\bar{t}H$ and $t\bar{t}Z$ processes can be measured with a percent-level statistical precision. Assuming negligible beyond-the-SM contamination in the $t\bar{t}Z$ production process, and in view of the theoretical systematics discussed in Section 2, this gives a measurement of the product of y_t times the $H \rightarrow b\bar{b}$ branching ratio, $B(H \rightarrow b\bar{b})$, to 1%. If the 100 TeV pp collider will be preceded by an e^+e^- collider, $B(H \rightarrow b\bar{b})$ may be known to better than 1% [24, 25, 12, 26], providing a direct measurement of y_t . If not, this result will likely provide the most precise constraint on a combination of Higgs couplings directly sensitive to y_t .

2. Theoretical systematics for the $t\bar{t}H/t\bar{t}Z$ production rate

It is well known that one of the key obstacles to exploiting the immense statistics available at hadron colliders for precision measurements, is the intrinsic difficulty in performing accurate absolute rate predictions. This difficulty arises from several sources. On one side we have the complexity, and often the large size, of higher-order contributions. At NLO one is often left with uncertainties in the range of 10% (although these can be much larger, as in the case of Higgs or $b\bar{b}$ production, and more in general for processes dominated by gg initial states), uncertainties that can be reduced to the few-percent level, but not always, only with the inclusion of NNLO effects. On the other, there are uncertainties due to the knowledge of initial-state parton distribution functions (PDFs), which for gg processes range from several percent, to order-one factors in the case of very small or very large x values. Furthermore, the modeling of the realistic final states, including the description of hadronization and analysis cuts, which are required for the comparison with experimental data, require an additional layer of theoretical control, which very often cannot match the available precision of fully inclusive parton-level results. Finally, for specific processes, there are uncertainties due to the knowledge of input parameters (e.g. the value of the top or bottom mass, for processes involving these heavy quarks).

Over the past few years, we have witnessed nevertheless a staggering progress in the theoretical precision, addressing all aspects listed above [27]. A benchmark example is the recent completion [28] of the NNNLO calculation for the inclusive Higgs production in the $gg \rightarrow H$ channel, which, accompanied by the improved determination and consistency of the gluon PDF luminosities [29], has now reduced to about $3\%_{\text{NNNLO}} \oplus 3\%_{\text{PDF}}$ the current uncertainty on the total production rate for this milestone process. A similar precision has been achieved [30] in the case of the $t\bar{t}$ production rate, at NNLO. In view of these examples, it is premature to establish today what the theoretical systematics will be at the time a 100 TeV pp collider will be operating. It is reasonable to anticipate that, also thanks to the opportunities offered by the precise LHC measurements for the validation of theoretical calculations and for the improvement of the PDFs, within the next 10, 20 or 30 years all Higgs production processes will be known with theoretical accuracy at the level of 1% or below.

This notwithstanding, it is extremely useful to explore observables that can help improving even further the precision, by providing more robust confirmation of the systematics, and enabling measurements where the experimental systematics can be reduced to levels comparable to the theoretical ones. It is in this spirit that we propose, for the study of this paper, the ratio of the $t\bar{t}H$ to

$t\bar{t}Z$ cross sections, performed in fiducial regions of acceptance that make them suitable for a realistic experimental analysis. As we shall discuss here, the theoretical understanding of these processes, including NLO QCD [31, 32, 33] and EW [34, 35] corrections, and including the current knowledge of PDFs, allows already today to support an intrinsic overall theoretical accuracy at the percent level. This precision will certainly be consolidated, and further improved, by future developments. Today, this allows to start probing the experimental prospects of the 100 TeV collider, to put in perspective the role of precision Higgs measurements at a such a facility, and to provide useful performance benchmarks for the design of the future detectors. In this Section we shall motivate such accuracy claim. What will be learned, can also contribute to improve the expectations for future runs of the LHC, by improving the predictions for the relative size of the $t\bar{t}H$ signal and its irreducible $t\bar{t}Z$ background.

2.1. Total rates and ratios

The main observation motivating the interest in the study of the $t\bar{t}H/t\bar{t}Z$ ratio is the close analogy between the two processes. At leading order (LO) they are both dominated by the gg initial state, with the H or Z bosons emitted off the top quark. The $q\bar{q}$ -initiated processes, which at the 100 (13) TeV amount for $\lesssim 10\%$ ($\lesssim 30\%$) of the total rates, only differ in the possibility to radiate the Z boson from the light-quark initial state. The difference induced by this effect, as we shall see, is not large, and is greatly reduced at 100 TeV. At NLO, renormalization, factorization and cancellation of collinear and soft singularities will be highly correlated between the two processes, since the relevant diagrams have the same structure, due to the identity of the tree-level diagrams. This justifies correlating, in the estimate of the renormalization and factorization scale uncertainties, the scale choices made for $t\bar{t}H$ and $t\bar{t}Z$. The uncertainties due to the mass of the top quark are also obviously fully correlated between numerator and denominator. Furthermore, due to the closeness in mass of the Higgs and Z bosons and the ensuing similar size of the values of x probed by the two processes, and given that the choice of PDFs to be used in numerator and denominator in the scan over PDF sets must be synchronized, we expect a significant reduction in the PDF systematics for the ratio. Finally, the similar production kinematics (although not identical, as we shall show in the next Section), should guarantee a further reduction in the modeling of the final-state structure, like shower-induced higher-order corrections, underlying-event effects, hadronization, etc.

The above qualitative arguments are fully supported by the actual calculations. All results are obtained using the MADGRAPH5_AMC@NLO code [36], which includes both NLO QCD and EW corrections. The default parameter set used in this study is:

Parameter	value	Parameter	value
G_μ	$1.1987498350461625 \cdot 10^{-5}$	n_{lf}	5
m_t	173.3	y_t	173.3
m_W	80.419	m_Z	91.188
m_H	125.0	α^{-1}	128.930

MSTW2008 NLO [37] is the default PDF set and $\mu_R = \mu_F = \mu_0 = \sum_{f \in \text{final states}} m_{T,f}/2$ is the default for the central choice of renormalization and factorization scales, where $m_{T,f}$ is the transverse mass of the final particle f . This scale choice interpolates between the dynamical scales that were shown in Ref. [31] to minimize the p_T dependence of the NLO/LO ratios for the top and Higgs spectra.

	$\sigma(t\bar{t}H)[\text{pb}]$	$\sigma(t\bar{t}Z)[\text{pb}]$	$\frac{\sigma(t\bar{t}H)}{\sigma(t\bar{t}Z)}$
13 TeV	$0.475^{+5.79\%+3.33\%}_{-9.04\%-3.08\%}$	$0.785^{+9.81\%+3.27\%}_{-11.2\%-3.12\%}$	$0.606^{+2.45\%+0.525\%}_{-3.66\%-0.319\%}$
100 TeV	$33.9^{+7.06\%+2.17\%}_{-8.29\%-2.18\%}$	$57.9^{+8.93\%+2.24\%}_{-9.46\%-2.43\%}$	$0.585^{+1.29\%+0.314\%}_{-2.02\%-0.147\%}$

Table 1: Total cross sections $\sigma(t\bar{t}H)$ and $\sigma(t\bar{t}Z)$ and the ratios $\sigma(t\bar{t}H)/\sigma(t\bar{t}Z)$ with NLO QCD corrections at 13 TeV and 100 TeV. Results are presented together with the renormalization/factorization scale and PDF+ α_s uncertainties.

		$\sigma(t\bar{t}H)[\text{pb}]$	$\sigma(t\bar{t}Z)[\text{pb}]$	$\frac{\sigma(t\bar{t}H)}{\sigma(t\bar{t}Z)}$
13 TeV	MSTW2008	$0.475^{+5.79\%+2.02\%}_{-9.04\%-2.50\%}$	$0.785^{+9.81\%+1.93\%}_{-11.2\%-2.39\%}$	$0.606^{+2.45\%+0.216\%}_{-3.66\%-0.249\%}$
	CT10	$0.450^{+5.70\%+6.00\%}_{-8.80\%-5.34\%}$	$0.741^{+9.50\%+5.91\%}_{-10.9\%-5.29\%}$	$0.607^{+2.34\%+0.672\%}_{-3.47\%-0.675\%}$
	NNPDF2.3	$0.470^{+5.26\%+2.22\%}_{-8.58\%-2.22\%}$	$0.771^{+8.97\%+2.16\%}_{-10.6\%-2.16\%}$	$0.609^{+2.23\%+0.205\%}_{-3.41\%-0.205\%}$
100 TeV	MSTW2008	$33.9^{+7.06\%+0.94\%}_{-8.29\%-1.26\%}$	$57.9^{+8.93\%+0.90\%}_{-9.46\%-1.20\%}$	$0.585^{+1.29\%+0.0526\%}_{-2.02\%-0.0758\%}$
	CT10	$32.4^{+6.87\%+2.29\%}_{-8.11\%-2.95\%}$	$55.5^{+8.73\%+2.16\%}_{-9.27\%-2.78\%}$	$0.584^{+1.27\%+0.189\%}_{-1.99\%-0.260\%}$
	NNPDF2.3	$33.2^{+6.62\%+0.78\%}_{-6.47\%-0.78\%}$	$56.9^{+7.62\%+0.75\%}_{-7.29\%-0.75\%}$	$0.584^{+1.29\%+0.0493\%}_{-2.01\%-0.0493\%}$

Table 2: Results with NLO QCD corrections at 13 TeV and 100 TeV, using three different sets of PDF. Results are presented together with the renormalization/factorization scale and PDF uncertainties. Contrary to Table 1, the α_S systematics is not included here.

We start by discussing the results at the LO in the EW effects. The scale variation is performed over the standard range $0.5\mu_0 \leq \mu_{R,F} \leq 2\mu_0$, with μ_R and μ_F varying independently. Both scale and PDF choices are correlated between numerator and denominator when taking the ratios. The resulting scale and MSTW 2008NLO PDF $+\alpha_S$ uncertainties, for the total cross sections of the individual processes and of for the ratio, are shown in Table 1. Notice that the scale uncertainty of the individual processes, in the range of $\pm 7 - 10\%$, is reduced to $\pm 1.5\%$ ($\pm 3\%$) for the ratios at 100 (13) TeV. The PDF variation is reduced by a factor close to 10, to the few permille level.

To corroborate the great stability of the ratios, we also consider different PDF sets, showing in Table 2 the results obtained using the following LHAPDF 5.9.1 [38] sets: MSTW2008 NLO [37], CT10 NLO [39] and NNPDF2.3 NLO [40] (in this case, we only consider the PDF variation, and not the α_S systematics). While the overall envelope of the predictions for the individual rates includes a $\pm 5\%$ range, the ratio uncertainty due to the PDFs remains at the few permille level.

We explore further variations in our default parameter set in Table 3. There, we remove the PDF uncertainties, which are practically unaffected by these parameter changes. Choosing the fixed value $\mu_0 = m_t + m_{H,Z}/2$ for the central choice of the renormalization and factorization scales, modifies the ratio $\sigma(t\bar{t}H)/\sigma(t\bar{t}Z)$ by $1\% - 1.5\%$, consistent with the range established using the dynamical scale.

For m_t , we consider a variation in the range of $m_t = 173.3 \pm 0.8$ GeV. We notice that $\sigma(t\bar{t}H)$ is practically constant. This is due to the anti-correlation between the increase (decrease) in rate due to

		$\sigma(t\bar{t}H)[\text{pb}]$	$\sigma(t\bar{t}Z)[\text{pb}]$	$\frac{\sigma(t\bar{t}H)}{\sigma(t\bar{t}Z)}$
13 TeV	default	$0.475^{+5.79\%}_{-9.04\%}$	$0.785^{+9.81\%}_{-11.2\%}$	$0.606^{+2.45\%}_{-3.66\%}$
	$\mu_0 = m_t + m_{H,Z}/2$	$0.529^{+5.96\%}_{-9.42\%}$	$0.885^{+9.93\%}_{-11.6\%}$	$0.597^{+2.45\%}_{-3.61\%}$
	$m_t = y_tv = 174.1$ GeV	$0.474^{+5.74\%}_{-9.01\%}$	$0.773^{+9.76\%}_{-11.2\%}$	$0.614^{+2.45\%}_{-3.66\%}$
	$m_t = y_tv = 172.5$ GeV	$0.475^{+5.81\%}_{-9.05\%}$	$0.795^{+9.82\%}_{-11.2\%}$	$0.597^{+2.45\%}_{-3.65\%}$
	$m_H = 126.0$ GeV	$0.464^{+5.80\%}_{-9.04\%}$	$0.785^{+9.81\%}_{-11.2\%}$	$0.593^{+2.42\%}_{-3.62\%}$
100 TeV	default	$33.9^{+7.06\%}_{-8.29\%}$	$57.9^{+8.93\%}_{-9.46\%}$	$0.585^{+1.29\%}_{-2.02\%}$
	$\mu_0 = m_t + m_{H,Z}/2$	$39.0^{+9.76\%}_{-9.57\%}$	$67.2^{+10.9\%}_{-10.6\%}$	$0.580^{+1.16\%}_{-1.80\%}$
	$m_t = y_tv = 174.1$ GeV	$33.9^{+7.01\%}_{-8.27\%}$	$57.2^{+8.90\%}_{-9.42\%}$	$0.592^{+1.27\%}_{-2.00\%}$
	$m_t = y_tv = 172.5$ GeV	$33.7^{+6.99\%}_{-8.31\%}$	$58.6^{+8.93\%}_{-9.46\%}$	$0.576^{+1.27\%}_{-1.99\%}$
	$m_H = 126.0$ GeV	$33.2^{+7.04\%}_{-8.28\%}$	$57.9^{+8.93\%}_{-9.46\%}$	$0.575^{+1.25\%}_{-1.95\%}$

Table 3: Results with NLO QCD corrections at 13 TeV and 100 TeV by varying some parameter values. Results are presented together with the renormalization/factorization scale uncertainties.

		$\sigma(t\bar{t}H)$ [pb]	$\sigma(t\bar{t}Z)$ [pb]	$\frac{\sigma(t\bar{t}H)}{\sigma(t\bar{t}Z)}$
13 TeV	$m_t = 174.1$ GeV	0.3640	0.5307	0.6860
	$m_t = 172.5$ GeV	0.3707	0.5454	0.6800
100 TeV	$m_t = 174.1$ GeV	23.88	37.99	0.629
	$m_t = 172.5$ GeV	24.21	38.73	0.625

Table 4: LO results at at TeV and 100 TeV, keeping the top Yukawa coupling $y_t v = 173.3$ GeV.

pure phase-space, and the decrease (increase) in the strength of y_t , when the top mass is lower (higher). The $t\bar{t}Z$ process is vice versa directly sensitive to m_t at the level of $\pm 1.5\%$ over the ± 0.8 GeV range, and this sensitivity is reflected in the variation of the cross-section ratio. We notice, however, that if we kept the value of y_t fixed when we change m_t , the dynamical effect on the rate would be totally correlated, and the ratio would remain constant to within a few permille, as shown in Table 4. This shows that the ratio is only sensitive to the strength of y_t , and only minimally to the precise value of m_t .

Finally, we observe a $\sim 2\%$ shift in $\sigma(t\bar{t}H)$ (and therefore in the ratios) when m_H is changed by 1 GeV, which is a gross underestimate of the precision with which the Higgs mass is [43] and will soon be known.

The effect of the NLO EW corrections in the $\alpha(m_Z)$ scheme is shown in Table 5. The shift in the ratio with respect to the pure NLO QCD result is of the order of 2%. For reference, we also provide the results in the G_μ scheme. In this scheme, we use $\alpha^{-1} = 132.50699632834286$ and $G_\mu = 1.166390 \cdot 10^{-5}$. The overall difference from the $\alpha(m_Z)$ scheme for the individual rates is at the percent level, and at the permille level for the ratios. We conclude that, once the known NLO EW effects are incorporated, the residual uncertainty of the cross-section ratio due to higher-order EW corrections should be significantly below the percent level.

Before closing this discussion of the total rates, we remark on the relation between the predictions for the cross section ratios at LO and at NLO. Since at LO the renormalization and factorization scales only appear in the PDFs and in $\alpha_s(\mu_R)$, and given that the numerical values of the scales is very similar (as a result of $m_H - m_Z \ll 2m_t + m_{H,Z}$), the LO ratios come with an unreliably optimistic estimate of the scale and PDF uncertainty. It is only at NLO that, through the introduction of the appropriate

		$\alpha(m_Z)$ scheme			G_μ scheme		
		$\sigma(t\bar{t}H)$ [pb]	$\sigma(t\bar{t}Z)$ [pb]	$\frac{\sigma(t\bar{t}H)}{\sigma(t\bar{t}Z)}$	$\sigma(t\bar{t}H)$ [pb]	$\sigma(t\bar{t}Z)$ [pb]	$\frac{\sigma(t\bar{t}H)}{\sigma(t\bar{t}Z)}$
13 TeV	NLO QCD	0.475	0.785	0.606	0.462	0.763	0.606
	$\mathcal{O}(\alpha_S^2 \alpha^2)$ Weak	-0.006773	-0.02516		0.004587	-0.007904	
	$\mathcal{O}(\alpha_S^2 \alpha^2)$ EW	-0.0045	-0.022		0.0071	-0.0033	
	NLO QCD+Weak	0.468	0.760	0.617	0.467	0.755	0.619
	NLO QCD+EW	0.471	0.763	0.617	0.469	0.760	0.618
100 TeV	NLO QCD	33.9	57.9	0.585	32.9	56.3	0.585
	$\mathcal{O}(\alpha_S^2 \alpha^2)$ Weak	-0.7295	-2.146		0.0269	-0.8973	
	$\mathcal{O}(\alpha_S^2 \alpha^2)$ EW	-0.65	-2.0		0.14	-0.77	
	NLO QCD+Weak	33.1	55.8	0.594	32.9	55.4	0.594
	NLO QCD+EW	33.2	55.9	0.594	33.1	55.6	0.595

Table 5: Effect of the EW NLO corrections, in the $\alpha(m_Z)$ and G_μ schemes, at 13 TeV and 100 TeV.

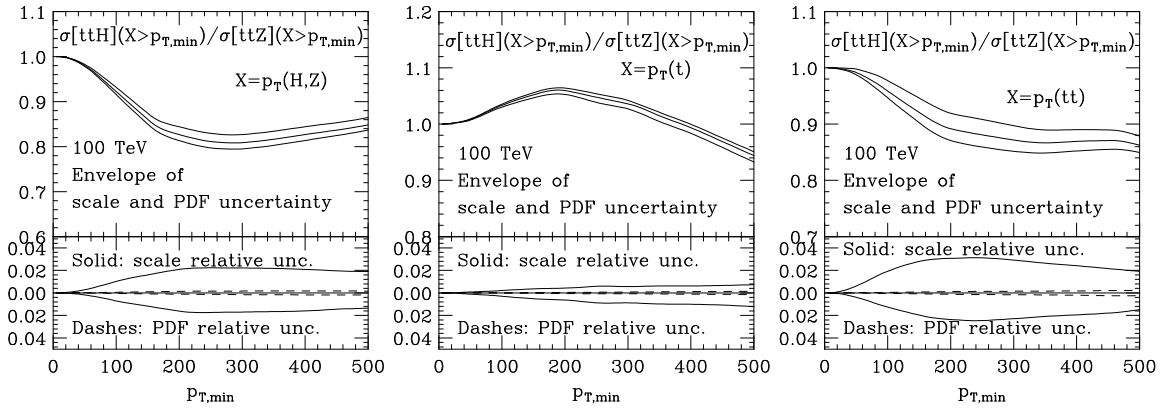


Figure 2: Scale and PDF systematics of ratios of integrated p_T spectra for different observables, at 100 TeV. From left to right: p_T of the boson, p_T of the top quark, p_T of the $t\bar{t}$ pair.

kinematical factors Q^2 in the renormalization logarithms $\log(\mu_R^2/Q^2)$, the relevant differences between the scale behavior of two processes are first exposed. At NLO one also encounters classes of (IR- and UV-finite) diagrams that differ between the two processes, and contribute to finite NLO terms that cannot be estimated using scale-variation arguments. For example, light-quark loops can couple to the Z boson, but not to the Higgs.

As always when using scale-variation tests to assess the theoretical systematics, there is therefore no guarantee that yet higher-order corrections will not exceed the range predicted by those estimates. For a measurement as important as the extraction of the top Yukawa coupling, it is reasonable to demand that the uncertainty estimates we provided here be confirmed by a full NNLO calculation, something that will certainly be possible over the next few years. Nevertheless we believe that the studies presented here provide a rather compelling case to argue that a precision at the percent level is reasonable.

2.2. Kinematical distributions

Any experimental analysis, and in particular the boosted approach that we employ in this work, will restrict the phase-space available to the final states. To preserve the precision in the theoretical prediction of the ratio of total $t\bar{t}H$ and $t\bar{t}Z$ cross sections, it is crucial to ensure that the reduction in systematic uncertainties carries over to the description of final states after kinematical cuts have been applied. We present here a summary of our studies at 100 TeV, focused on the kinematical distributions most relevant for our studies, and limited to main sources of uncertainty (scale and PDF). The results for other distributions and for other systematics (top mass, EW scheme), at 100 and at 13 TeV, lead to similar results, and are available upon request.

We show in Fig. 2 the ratio of the integrated p_T spectra of various final-state objects X : $\sigma[t\bar{t}H](p_{T,X} > p_{T,\min}) / \sigma[t\bar{t}Z](p_{T,X} > p_{T,\min})$. On the left, $X = H(Z)$ for the $t\bar{t}H$ ($t\bar{t}Z$) process. In the middle, $X = t$ and on the right X is the $t\bar{t}$ system. We normalize the ratios to 1 at $p_{T,\min} = 0$, so that the resulting uncertainties correspond to the systematics in the extrapolation of the ratio of differential distributions to the ratio of the total rates. The three upper panels show that the ratios are not a constant, and can change by up to 20% up to $p_T = 500$ GeV. The relative uncertainties, separately for the scale and PDF variation (MSTW2008 NLO set), are shown in the lower plots. The scale uncertainties reach a value of $\pm 2\%$ for the boson p_T spectra, $\pm 1\%$ for the top, and $\pm 3\%$ for the p_T of the $t\bar{t}$ pair. The PDF uncertainties remain well below the percent level throughout.

These results imply that the relative shapes of the p_T spectra can be controlled with a precision that remains consistent with the overall goal of a percent-level extraction of the relative rates. There is no doubt that future NNLO calculations of both processes will improve this even further. Very precise measurements of the shape of the Z boson spectra in $t\bar{t}Z$ events using e.g. the very clean leptonic Z decay will also help confirming the accuracy of the predicted p_T spectra and reduce a possible left-over uncertainty.

3. Boosted $t\bar{t}H$ at 100 TeV

Just like at the LHC, the $t\bar{t}H$ production process can be studied for a variety of Higgs decay channels. We collect in Table 6 the event rates for potentially interesting Higgs decays combined with $t\bar{t}H$ production, for an integrated luminosity of 20 ab^{-1} at 100 TeV. These numbers include the branching ratio for the mixed lepton-hadron $t\bar{t} \rightarrow \ell\nu_\ell + \text{jets}$ decay ($\ell = e, \mu$), in addition to the relevant Higgs branching ratios.

Considering that analysis cuts and efficiencies will typically reduce these rates by a further factor of 10 or more, it is clear that the otherwise very clean $H \rightarrow 4\ell$ does not have the minimum number of 10^4 events, required to aim for a 1% target precision. In the case of $H \rightarrow \gamma\gamma$ (see also [44]), we considered a simple parton-level analysis, implementing basic cuts such as:

$$\begin{aligned} p_{T,\gamma,b,j} > 25 \text{ GeV} , & \quad |\eta_{\gamma,b,j}| < 2.5 , & \quad \Delta R_{jj,bb,bj} > 0.4 \\ p_{T,\ell} > 20 \text{ GeV} , & \quad |\eta_\ell| < 2.5 \end{aligned} \quad (1)$$

These leave around $5 \cdot 10^4$ events with 20 ab^{-1} , while the $t\bar{t}\gamma\gamma$ background, subject to a $|m_{\gamma\gamma} - 125| < 5 \text{ GeV}$ cut, is almost a factor of 10 smaller. On the other hand, detection efficiencies, such as those related to lepton or photon isolation and to b tagging, make this channel borderline for a 1% statistical accuracy, and call for a dedicated study including realistic projections of detector performance. The $H \rightarrow 2\ell 2\nu$ final state has a potentially interesting rate, which may deserve a separate study.

Given the extraordinary rate for the $H \rightarrow b\bar{b}$ final state, and following the original LHC analysis [6], we focus on this channel,

$$pp \rightarrow t\bar{t}H \rightarrow (bjj) (\bar{b}\ell\bar{\nu}) (b\bar{b}), (b\ell\nu) (\bar{b}jj) (b\bar{b}) . \quad (2)$$

The leptonic top decay guarantees the triggering and reduces multi-jet combinatorics. The leading backgrounds are:

- $pp \rightarrow t\bar{t}b\bar{b}$, the main irreducible QCD background
- $pp \rightarrow t\bar{t}Z$, including the Z -peak in the m_{bb} distribution
- $pp \rightarrow t\bar{t}$ +jets with fake-bottoms tags

Additional backgrounds like W +jets will be small and do not lead to dangerous kinematical features for our analysis [6]. The analysis strategy based on boosted top and Higgs decays is extremely simple [6],

- (i) an isolated lepton
- (ii) a tagged top without any b -tag requirement
- (iii) a tagged Higgs with two b -tags inside
- (iv) a continuum b -tag outside the top and Higgs fat jets

The m_{bb} distribution will provide us with simple sidebands to control the $t\bar{t}b\bar{b}$ and $t\bar{t}$ +jets backgrounds, and a second mass peak from the $t\bar{t}Z$ mass peak. We discuss the unfortunate need for the continuum b -tag below. The simplicity of our analysis will allow us to efficiently control systematics.

For simplicity, all Monte Carlo event samples are generated at leading order. The main effects from the available higher order predictions of the $t\bar{t}H$ signal [31, 32], the $t\bar{t}Z$ background [33], the $t\bar{t}b\bar{b}$ background [42], and the $t\bar{t}$ +jets background [45] are discussed separately in Section 2, so for the signal-background analysis we leave them out. We use MADGRAPH5 [46] with NNPDF23 parton densities [47], showering and hadronization via PYTHIA8 [48] and the fast detector simulation with DELPHES3 [49, 50].

$H \rightarrow 4\ell$	$H \rightarrow \gamma\gamma$	$H \rightarrow 2\ell 2\nu$	$H \rightarrow b\bar{b}$
$2.6 \cdot 10^4$	$4.6 \cdot 10^5$	$2.0 \cdot 10^6$	$1.2 \cdot 10^8$

Table 6: $t\bar{t}H$ event rates for various Higgs decay modes, with 20 ab^{-1} at 100 TeV, assuming $t\bar{t} \rightarrow \ell\nu + \text{jets}$. Here and for Higgs decays, ℓ can be either an electron or a muon.

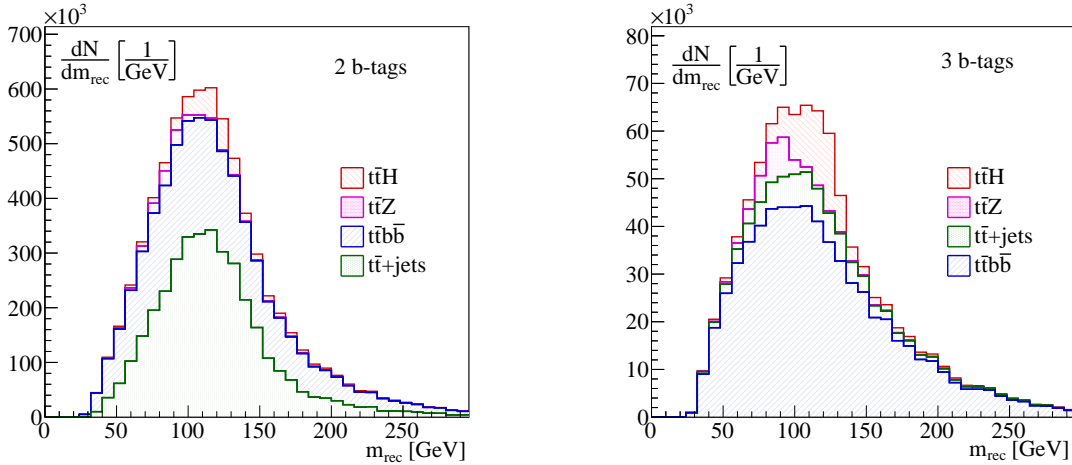


Figure 3: Reconstructed m_{bb} for the leading- J substructures in the fat Higgs jet. We require two b -tags inside the fat Higgs jet (left) and an additional continuum b -tag (right). The event numbers are scaled to $\mathcal{L} = 20 \text{ ab}^{-1}$.

At the generator level we require $p_{T,j,b,\ell} > 10 \text{ GeV}$ and $\Delta R_{jj,bb,j\ell} > 0.1$. The $t\bar{t}$ +jets background is generated as one hard jet with $p_{T,j} > 100 \text{ GeV}$ at the hard matrix element level. We do not consider merged samples since we found that the influence of $t\bar{t} + 2j$ to our analysis is negligible. After generator cuts we start with a signal cross section of 4.2 pb. Associated $t\bar{t}Z$ production yields 1.2 pb. The continuum $t\bar{t}b\bar{b}$ background counts 121 pb and is at this stage dominated by $t\bar{t}$ +jets with 2750 pb.

DELPHES3 provides isolated leptons as well as parton-level b -quarks needed for the tagging procedure later-on. Leptons have to pass a minimum $p_{T,\ell} > 10 \text{ GeV}$. For their isolation we demand a transverse momentum ratio (isolation variable) of $I < 0.1$ within $\Delta R < 0.3$. Finally, we use the energy flow objects for hadrons to cluster via the Cambridge/Aachen (C/A) jet algorithm [51]. The jet clustering and the analysis are done with FASTJET3 [52], a modified BDRS Higgs tagger [23, 6] and the HEPTOPTAGGER2 [22]. For all b -tags we require a parton-level b -quark within $\Delta R < 0.3$.

First, we require one isolated lepton with $|y_\ell| < 2.5$ and $p_{T,\ell} > 15 \text{ GeV}$. For the top tag [53, 54, 55], we cluster the event into fat C/A jets with $R = 1.8$ and $p_{T,j} > 200 \text{ GeV}$. Provided we find at least two fat jets we apply the HEPTOPTAGGER2 with the kinematic requirement $|y_j^{(t)}| < 4$. The recent significant update of the HEPTOPTAGGER2 relies on two additional pieces of information to achieve a significant improvement [22]. One of them is N -subjettiness [56], which adds some sensitivity to the color structure of the event. The other is the optimalR mode, which based on a constant fat jet mass reduces the size of the fat jet [57] to the point where the fat jet stops containing all hard top decay subjets. This minimal size can also be computed based on the transverse momentum of the fat jet. Since the signal and all considered backgrounds include a hadronic top quark, changing the top tagging parameters results only in an overall scaling factor. In this analysis we do not cut on the difference between the expected and the found optimal radius because the initial fat jet size is already chosen to fit the expected transverse momenta. To have a handle on the QCD multi-jet background, we place a mild cut on the filtered N -subjettiness ratio $\tau_3/\tau_2 < 0.8$ which can be tightened at the cost of signal efficiency if desired. After identifying the boosted top we remove the associated hadronic activity and apply a modified BDRS Higgs tagger to fat C/A jet(s) with $R = 1.2$, $|y_j^{(H)}| < 2.5$, and $p_{T,j} > 200 \text{ GeV}$. Our decomposition of the fat jet into hard substructure includes a cutoff of $m_{\text{sub}} > 40 \text{ GeV}$ for the relevant substructure and a mass drop threshold of 0.9. The hard substructures are then paired in all possible ways and ordered by their modified Jade distance,

$$J = p_{T,1} p_{T,2} (\Delta R_{12})^4. \quad (3)$$

The leading pairing we filter [23] including the three hardest substructures, to allow for hard gluon radiation. For consistency we require a reconstructed transverse momentum above 200 GeV. Within

$m_{bb} \in [100, 150]$ GeV	2 b -tags	3 b -tags	ratio
$t\bar{t}H$	2.4E+5	6.4E+4	1/3.8
$t\bar{t}b\bar{b}$	1.2E+6	2.4E+5	1/5.0
$t\bar{t}$ + jets	1.9E+6	3.8E+4	1/50
$t\bar{t}Z$	2.3E+4	4.9E+3	1/4.7

Table 7: Event rates assuming an integrated luminosity of 20 ab^{-1} .

this Higgs candidate we ask for two b -tags, assuming a global tagging efficiency of 50% and a mis-tagging probability of 1% for all jets within $|y_j| < 2.5$ and $p_{T,j} > 30$ GeV. As we can see in the left panel of Fig. 3, the $t\bar{t}$ +jets and $t\bar{t}b\bar{b}$ backgrounds are of similar size at this stage. Moreover, the analysis sculpts the backgrounds towards $m_{bb} \sim 100$ GeV.

To simplify the background composition and to avoid the strong background sculpting it turns out that a third, continuum b -tag is useful. We target the decay jet of the otherwise leptonically decaying top by removing the top and Higgs constituents from the event and then clustering the remaining hadronic structure into C/A jets with $R = 0.6$ and $p_{T,j} > 30$ GeV. For one of them we require a b -tag within $|y_b| < 2.5$ and an angular separation $\Delta R_{b,j} > 0.4$ from all other jets, now including the top and Higgs decay products.

The effect of this third b -tag becomes clear in the right panel of Fig. 3. We are now dominated by the continuum $t\bar{t}b\bar{b}$ background. The corresponding event rates for an integrated luminosity of 20 ab^{-1} are given in Tab. 7. While the light-flavor $t\bar{t}$ +jets background is now suppressed well below the leading $t\bar{t}b\bar{b}$ background it is still of the same size as the Higgs signal, which means we still need to include it in our analysis.

4. Updated BDRS tagger

The two improvements of the HEPTOPTAGGER2 can also be added to the BDRS Higgs tagger [23, 52, 58]. The decay $H \rightarrow b\bar{b}$ will typically contain two hard substructures, so using N -subjettiness the characteristic parameter τ_2/τ_1 has to be small. The correlations between the reconstructed masses and the ratio τ_2/τ_1 of the filtered fat jets in Fig. 4 indicate that a cut $\tau_2/\tau_1 < 0.4$ not only reduces the backgrounds but additionally leads to narrower and better-defined mass peaks for the Higgs and Z -decays as shown in Fig. 5.

In the optimalR version of the BDRS tagger we reduce the size of the Higgs fat jet candidate. Aside from reduced underlying event and pile-up this minimizes the combinatorics in the m_{bb} reconstructions. As for the top case [22] we shrink the fat jet radius in steps of 0.1 as long as the jet mass does not drop below $m_j < 0.8 m_{j,\text{orig}}$ relative to the originally tagged Higgs jet with $R = 1.2$. We can extract

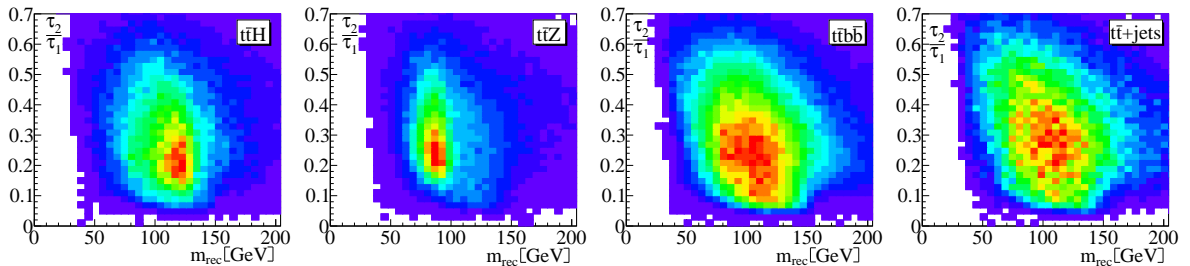


Figure 4: Correlation between the reconstructed mass m_{rec} and the N -subjettiness ratio τ_2/τ_1 of the filtered Higgs candidate fat jet for the signal and background samples. The event numbers are scaled to $\mathcal{L} = 20 \text{ ab}^{-1}$.

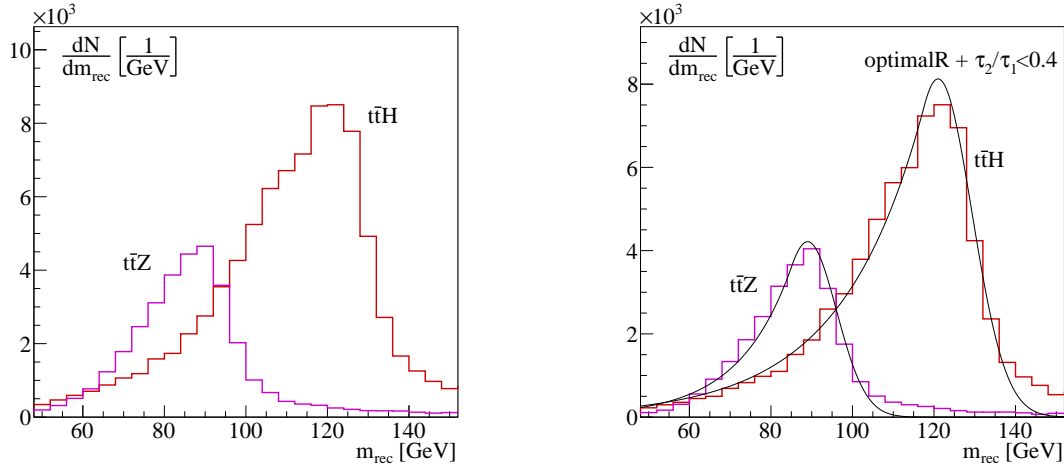


Figure 5: Reconstructed m_{bb} of the Higgs and Z candidates in $t\bar{t}H$ and $t\bar{t}Z$ production with the default BDRS tagger (left) and after using optimalR and the N -subjettiness cut $\tau_2/\tau_1 < 0.4$ (right). In the right panel we include the fitted Crystal Ball functions. The event numbers are scaled to $\mathcal{L} = 20 \text{ ab}^{-1}$.

the expected value of ΔR_{bb} from a fit to Monte Carlo simulations,

$$\Delta R_{bb}^{(\text{calc})} = \frac{250 \text{ GeV}}{p_{T,\text{filt}}} . \quad (4)$$

This supports the choice of $R = 1.2$ for the C/A jet clustering for the Higgs Tagger requiring transverse momenta of $p_T > 200 \text{ GeV}$. Unfortunately, for $t\bar{t}H$ production the relation between the expected and the measured values of ΔR_{bb} does not significantly improve the analysis. However, the mass difference between the Higgs and the Z boson leads to a shifted peak in the $\Delta R_{bb} - \Delta R_{bb}^{(\text{calc})}$ distribution for $t\bar{t}Z$. This shift allows for an additional reduction of $t\bar{t}Z$ if desired. In the final result shown in the left panel of Fig. 6 we include a triple b -tag, the N -subjettiness variable τ_2/τ_1 , and a modified fat jet radius for the Higgs candidate. Since the background region $m_{bb} \in [160, 300] \text{ GeV}$ is smooth and untouched by any signal, we can use it to subtract the QCD continuum from the combined $t\bar{t}H$ and $t\bar{t}Z$ signal. If the soft regime $m_{bb} \in [0, 60] \text{ GeV}$ can be useful in the same way needs to be checked by a full experimental analysis.

For the signal region $m_{bb} \in [104, 136] \text{ GeV}$ we arrive at a signal-to-background ratio around $S/B \approx 1/3$ and a Gaussian significance $S/\sqrt{B} = 120$, assuming an integrated luminosity of $\mathcal{L} = 20 \text{ ab}^{-1}$. The error on the number of nominally $N_S = 44700$ signal events is given by two terms. First, we assume that we can determine N_S from the total number of events $N_S + N_B$ using a perfect determination of N_B from the side bands. Second, the side band $m_{bb} \in [160, 296] \text{ GeV}$ with altogether $N_{\text{side}} = 135000$ events and a relative uncertainty of $1/\sqrt{N_{\text{side}}}$ introduces a statistical uncertainty ΔN_B , altogether leading to

$$\begin{aligned} \Delta N_S &= \left[\left(\sqrt{N_S + N_B} \right)^2 + (\Delta N_B)^2 \right]^{1/2} \\ &= \left[\left(\sqrt{N_S + N_B} \right)^2 + \left(\frac{N_B}{\sqrt{N_{\text{side}}}} \right)^2 \right]^{1/2} = 0.013 N_S . \end{aligned} \quad (5)$$

For the Yukawa coupling this translates into a relative error of around 1%. The first term alone would give $\Delta N_S = 0.010 N_S$.

In the right panel of Fig. 6 we show a combined fit to the Z and Higgs peaks assuming a perfect background subtraction. A combined analysis of both peaks (with known masses) serves as a check of the jet substructure techniques [23, 6] and as a means to reduce systematic and theoretical uncertainties, as discussed in Section 2. Given separate simulations for the Higgs and Z peaks, we

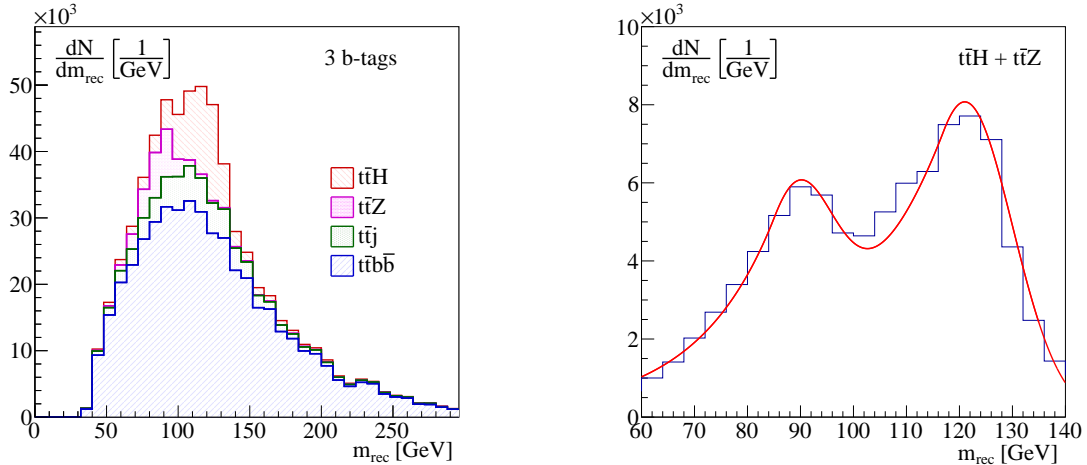


Figure 6: Left: Reconstructed m_{bb} for the leading- J substructures in the fat Higgs jet. We require two b -tags inside the fat Higgs jet and a continuum b -tag. Unlike in Fig. 3 we apply an N -subjettiness cut and use an optimalR version of the BDRS tagger. Right: Double-peak fit assuming perfect continuum background subtraction. The event numbers are scaled to $\mathcal{L} = 20 \text{ ab}^{-1}$.

can fix the shape of both distributions by fitting a Crystal Ball function [59] to each of them as done in the right panel of Fig. 5. For these fits we limit the exponent of the non-Gaussian tails to 50. In addition we fix the peak positions accounting for a shift due to losses in the reconstruction. Their linear combination allows us to model the background subtracted mass distribution. In the combined fit we keep all shape parameters fixed and allow only for separate scaling factors of each peak. From the double Crystal Ball function we finally receive the relative size of the two peak areas $N_H/N_Z = 2.80 \pm 0.03$. Using the combined fit therefore allows us to probe the top Yukawa coupling with a statistical precision of $\sim 0.5\%$. Given the discussion of Section 2, this precision can be eventually matched by the theoretical systematics, assuming no new physics affects $t\bar{t}Z$ production beyond the percent level. It remains to be explored to which extent the future detectors can benefit from the potential cancellations of experimental systematics in the measurement of the N_H/N_Z ratio.

5. Outlook

The top Yukawa coupling is one of two key parameter required for the understanding of the Higgs potential, and it is a crucial ingredient to the measurement of the Higgs self-coupling. At the LHC its determination will be limited to around $\Delta y_t/y_t \approx 10\%$ because of statistical as well as theoretical uncertainties [9, 5]. At a 100 TeV hadron collider the increased statistics will significantly improve this measurement.

We proposed here to measure the top Yukawa coupling using the decay $H \rightarrow b\bar{b}$ in the boosted phase space regime. Our simple analysis strategy [6] relies on a trigger lepton and two fat jets, one from the hadronic Higgs decay and one from the hadronic top decay. The m_{bb} distribution will show a clear peak from the Higgs signal as well as a similarly large peak from the Z background. The continuum side band and the second peak offer two ways to control the backgrounds as well as the translation of the $t\bar{t}b\bar{b}$ rate into a measurement of the Yukawa coupling. We find that a measurement of the top Yukawa coupling to around 1% should be feasible at 100 TeV collider energy with an integrated luminosity of 20 ab^{-1} . This is an order of magnitude improvement over the expected LHC reach, with significantly improved control over the critical uncertainties.

There exist additional, complementary handles on the uncertainties. For example, the $H \rightarrow \gamma\gamma$ decay could allow a direct measurement of the ratio of branching ratios $B(H \rightarrow \gamma\gamma)/B(H \rightarrow b\bar{b})$. It would serve as a complementary, although indirect, probe of the $t\bar{t}H$ coupling. Furthermore, $H \rightarrow 2\ell 2\nu$ could also be interesting, since there is enough rate to explore the regime $p_{T,H} \gg m_H$, which, particularly for the $e^\pm\mu^\mp\nu\bar{\nu}$ final state, could prove particularly clean.

Acknowledgments

TS would like to thank the International Max Planck Research School for *Precision Tests of Fundamental Symmetries* for their support. HSS would like to thank S. Frixione, V. Hirschi, D. Pagani and M. Zaro for useful discussions and for collaborating on the EW project in MADGRAPH5_AMC@NLO. The work of MLM and HSS is supported by the ERC grant 291377 *LHCtheory: Theoretical predictions and analyses of LHC physics: advancing the precision frontier*.

References

- [1] P. W. Higgs, Phys. Lett. **12**, 132 (1964); P. W. Higgs, Phys. Rev. Lett. **13**, 508 (1964); F. Englert and R. Brout, Phys. Rev. Lett. **13**, 321 (1964).
- [2] G. Aad *et al.* [ATLAS Collaboration], Phys. Lett. B **716**, 1 (2012), S. Chatrchyan *et al.* [CMS Collaboration], Phys. Lett. B **716**, 30 (2012).
- [3] see e.g. G. Degrandi, S. Di Vita, J. Elias-Miro, J. R. Espinosa, G. F. Giudice, G. Isidori and A. Strumia, JHEP **1208**, 098 (2012); S. Alekhin, A. Djouadi and S. Moch, Phys. Lett. B **716**, 214 (2012); L. A. Anchordoqui, I. Antoniadis, H. Goldberg, X. Huang, D. Lust, T. R. Taylor and B. Vlcek, JHEP **1302**, 074 (2013); D. Buttazzo, G. Degrandi, P. P. Giardino, G. F. Giudice, F. Sala, A. Salvio and A. Strumia, JHEP **1312**, 089 (2013); F. Bezrukov and M. Shaposhnikov, J. Exp. Theor. Phys. **120**, 335 (2015); A. Eichhorn, H. Gies, J. Jaeckel, T. Plehn, M. M. Scherer and R. Sondenheimer, JHEP **1504**, 022 (2015); F. Loebbert and J. Plefka, arXiv:1502.03093 [hep-ph].
- [4] For a comprehensive analysis of Run I data see e.g. T. Corbett, O. J. P. Eboli, D. Goncalves, J. Gonzalez-Fraile, T. Plehn and M. Rauch, arXiv:1505.05516 [hep-ph].
- [5] R. Brock *et al.*, arXiv:1401.6081 [hep-ex].
- [6] T. Plehn, G. P. Salam and M. Spannowsky, Phys. Rev. Lett. **104** (2010) 111801.
- [7] V. Khachatryan *et al.* [CMS Collaboration], JHEP **1409**, 087 (2014) [Erratum-ibid. **1410**, 106 (2014)]; G. Aad *et al.* [ATLAS Collaboration], Phys. Lett. B **740**, 222 (2015); V. Khachatryan *et al.* [CMS Collaboration], arXiv:1502.02485 [hep-ex].
- [8] V. Drollinger, T. Müller and D. Denegri, hep-ph/0111312; J. Cammin and M. Schumacher, ATLAS-2003-024; P. Artoisenet, P. de Aquino, F. Maltoni and O. Mattelaer, Phys. Rev. Lett. **111**, 091802 (2013); D. Curtin, J. Galloway and J. G. Wacker, Phys. Rev. D **88**, 093006 (2013); P. Agrawal, S. Bandyopadhyay and S. P. Das, Phys. Rev. D **88**, 093008 (2013); M. R. Buckley, T. Plehn, T. Schell and M. Takeuchi, JHEP **1402**, 130 (2014).
- [9] M. Klute, R. Lafaye, T. Plehn, M. Rauch and D. Zerwas, Europhys. Lett. **101**, 51001 (2013).
- [10] G. Weiglein *et al.* [LHC/LC Study Group Collaboration], Phys. Rept. **426**, 47 (2006); G. Moortgat-Pick *et al.*, arXiv:1504.01726 [hep-ph].
- [11] A. Ball *et al.*, Tech. Rep. FCC-ACC-SPC-0001.
- [12] <http://cepc.ihep.ac.cn/preCDR/volume.html>
- [13] For a general overview, see N. Arkani-Hamed, T. Han, M. L. Mangano, L.-T. Wang, to appear.
- [14] B. S. Acharya, K. Bozek, C. Pongkitivanichkul and K. Sakurai, JHEP **1502**, 181 (2015); S. Gori, S. Jung, L. T. Wang and J. D. Wells, JHEP **1412**, 108 (2014); J. Bramante, P. J. Fox, A. Martin, B. Ostdiek, T. Plehn, T. Schell and M. Takeuchi, Phys. Rev. D **91**, 054015 (2015); A. Berlin, T. Lin, M. Low and L. T. Wang, Phys. Rev. D **91**, no. 11, 115002 (2015); S. A. R. Ellis and B. Zheng, arXiv:1506.02644 [hep-ph].
- [15] T. G. Rizzo, Phys. Rev. D **89**, no. 9, 095022 (2014); A. Hook and A. Katz, JHEP **1409**, 175 (2014).
- [16] D. Curtin, P. Meade and C. T. Yu, JHEP **1411**, 127 (2014).
- [17] J. Hajer, Y. Y. Li, T. Liu and J. F. H. Shiu, arXiv:1504.07617 [hep-ph]; A. Freitas, S. Westhoff and J. Zupan, arXiv:1506.04149 [hep-ph].
- [18] U. Baur, T. Plehn and D. L. Rainwater, Phys. Rev. D **69**, 053004 (2004); A. J. Barr, M. J. Dolan, C. Englert, D. E. Ferreira de Lima and M. Spannowsky, JHEP **1502**, 016 (2015); A. V. Kotwal, S. Chekanov and M. Low, Phys. Rev. D **91**, no. 11, 114018 (2015). W. Yao, arXiv:1308.6302 [hep-ph]; H. J. He, J. Ren and W. Yao, arXiv:1506.03302 [hep-ph]; A. Azatov, R. Contino, G. Panico and M. Son, Phys. Rev. D **92**, no. 3, 035001 (2015).
- [19] M. Benedikt, talk at the FCC week 2015, Washington D.C., 23-29 March 2015, <http://indico.cern.ch/event/340703/session/108/contribution/186>; I. Hinchliffe, A. Kotwal, M. L. Mangano, C. Quigg and L. T. Wang, Int. J. Mod. Phys. A **30**, no. 23 (2015).
- [20] R. Lafaye, T. Plehn, M. Rauch, D. Zerwas and M. Dürrsen, JHEP **0908**, 009 (2009); K. Cranmer, S. Kreiss, D. Lopez-Val and T. Plehn, Phys. Rev. D **91**, no. 5, 054032 (2015).
- [21] J. R. Christiansen and T. Sjöstrand, JHEP **1404**, 115 (2014); F. Krauss, P. Petrov, M. Schoenherr and M. Spannowsky, Phys. Rev. D **89**, no. 11, 114006 (2014); T. Cohen, R. T. D'Agnolo, M. Hance, H. K. Lou and J. G. Wacker, JHEP **1411**, 021 (2014); A. J. Larkoski and J. Thaler, Phys. Rev. D **90**, no. 3, 034010 (2014); T. Han, J. Sayre and S. Westhoff, JHEP **1504**, 145 (2015); J. A. Aguilar-Saavedra, B. Fuks and M. L. Mangano, Phys. Rev. D **91**, 094021 (2015); A. J. Larkoski, F. Maltoni and M. Selvaggi, JHEP **1506**, 032 (2015); M. Spannowsky and M. Stoll, arXiv:1505.01921 [hep-ph]; G. Perez, Y. Soreq, E. Stamou and K. Tobioka, arXiv:1505.06689 [hep-ph].
- [22] G. Kasieczka, T. Plehn, T. Schell, T. Strebler and G. P. Salam, arXiv:1503.05921 [hep-ph].
- [23] J. M. Butterworth, A. R. Davison, M. Rubin and G. P. Salam, Phys. Rev. Lett. **100**, 242001 (2008).
- [24] K. Fujii *et al.*, arXiv:1506.05992 [hep-ex].
- [25] M. Bicer *et al.* [TLEP Design Study Working Group Collaboration], JHEP **1401**, 164 (2014).
- [26] L. Linssen, A. Miyamoto, M. Stanitzki and H. Weerts, arXiv:1202.5940 [physics.ins-det].

- [27] S. Dittmaier *et al.* [LHC Higgs Cross Section Working Group Collaboration], arXiv:1101.0593 [hep-ph], arXiv:1201.3084 [hep-ph].
- [28] C. Anastasiou, C. Duhr, F. Dulat, F. Herzog and B. Mistlberger, Phys. Rev. Lett. **114**, 212001 (2015).
- [29] J. Rojo *et al.*, arXiv:1507.00556 [hep-ph].
- [30] M. Czakon, P. Fiedler and A. Mitov, Phys. Rev. Lett. **110**, 252004 (2013).
- [31] W. Beenakker, S. Dittmaier, M. Krämer, B. Plümper, M. Spira and P. M. Zerwas, Nucl. Phys. B **653**, 151 (2003); S. Dawson, C. Jackson, L. H. Orr, L. Reina and D. Wackerth, Phys. Rev. D **68**, 034022 (2003).
- [32] A. Denner and R. Feger, arXiv:1506.07448 [hep-ph].
- [33] A. Lazopoulos, T. McElmurry, K. Melnikov and F. Petriello, Phys. Lett. B **666**, 62 (2008).
- [34] S. Frixione, V. Hirschi, D. Pagani, H. S. Shao and M. Zaro, JHEP **1409**, 065 (2014).
- [35] S. Frixione, V. Hirschi, D. Pagani, H.-S. Shao and M. Zaro, JHEP **1506**, 184 (2015).
- [36] J. Alwall *et al.*, JHEP **1407**, 079 (2014).
- [37] A. D. Martin, W. J. Stirling, R. S. Thorne and G. Watt, Eur. Phys. J. C **63**, 189 (2009).
- [38] M. R. Whalley, D. Bourilkov and R. C. Group, hep-ph/0508110.
- [39] H. L. Lai, M. Guzzi, J. Huston, Z. Li, P. M. Nadolsky, J. Pumplin and C.-P. Yuan, Phys. Rev. D **82**, 074024 (2010).
- [40] R. D. Ball *et al.*, Nucl. Phys. B **867**, 244 (2013).
- [41] R. Frederix, S. Frixione, V. Hirschi, F. Maltoni, R. Pittau and P. Torrielli, JHEP **1202**, 099 (2012).
- [42] A. Bredenstein, A. Denner, S. Dittmaier and S. Pozzorini, Phys. Rev. Lett. **103**, 012002 (2009); A. Bredenstein, A. Denner, S. Dittmaier and S. Pozzorini, JHEP **1003**, 021 (2010); G. Bevilacqua, M. Czakon, C. G. Papadopoulos, R. Pittau and M. Worek, JHEP **0909**, 109 (2009).
- [43] G. Aad *et al.* [ATLAS and CMS Collaborations], Phys. Rev. Lett. **114**, 191803 (2015).
- [44] F. Maltoni, D. Pagani and I. Tsinikos, arXiv:1507.05640 [hep-ph].
- [45] G. Bevilacqua, M. Czakon, C. G. Papadopoulos and M. Worek, Phys. Rev. Lett. **104**, 162002 (2010).
- [46] J. Alwall, M. Herquet, F. Maltoni, O. Mattelaer and T. Stelzer, JHEP **1106**, 128 (2011).
- [47] R. D. Ball *et al.* [NNPDF Collaboration], Nucl. Phys. B **877**, 290 (2013).
- [48] T. Sjöstrand, S. Ask, J. R. Christiansen, R. Corke, N. Desai, P. Ilten, S. Mrenna and S. Prestel *et al.*, Comput. Phys. Commun. **191** (2015) 159.
- [49] M. Selvaggi, J. Phys. Conf. Ser. **523** (2014) 012033.
- [50] J. Anderson, A. Avetisyan, R. Brock, S. Chekanov, T. Cohen, N. Dhirra, J. Dolen and J. Hirschauer *et al.*, arXiv:1309.1057 [hep-ex]. Detector card adapted for DELPHES3.2.
- [51] Y. L. Dokshitzer, G. D. Leder, S. Moretti and B. R. Webber, JHEP **9708**, 001 (1997); M. Wobisch and T. Wengler, In “Hamburg 1998/1999, Monte Carlo generators for HERA physics” 270-279. [hep-ph/9907280].
- [52] M. Cacciari and G. P. Salam, Phys. Lett. B **641**, 57 (2006); M. Cacciari, G. P. Salam and G. Soyez, Eur. Phys. J. C **72**, 1896 (2012).
- [53] K. Agashe *et al.* Phys. Rev. D **77**, 015003 (2008); G. Brooijmans, ATL-PHYS-CONF-2008-008 and ATL-COM-PHYS-2008-001, Feb. 2008 J. Thaler and L. T. Wang, JHEP **0807**, 092 (2008); D. E. Kaplan, K. Rehermann, M. D. Schwartz and B. Tweedie, Phys. Rev. Lett. **101**, 142001 (2008); L. G. Almeida *et al.*, Phys. Rev. D **79**, 074017 (2009); L. G. Almeida *et al.*, Phys. Rev. D **79**, 074012 (2009).
- [54] T. Plehn, M. Spannowsky, M. Takeuchi and D. Zerwas, JHEP **1010**, 078 (2010); C. Anders, C. Bernaciak, G. Kasieczka, T. Plehn and T. Schell, Phys. Rev. D **89**, no. 7, 074047 (2014).
- [55] M. H. Seymour, Z. Phys. C **62**, 127 (1994); T. Plehn and M. Spannowsky, J. Phys. G **39**, 083001 (2012); A. Abdesselam *et al.*, Eur. Phys. J. C **71**, 1661 (2011); A. Altheimer *et al.*, J. Phys. G **39**, 063001 (2012).
- [56] J. Thaler and K. Van Tilburg, JHEP **1103**, 015 (2011); J. Thaler and K. Van Tilburg, JHEP **1202**, 093 (2012); I. W. Stewart, F. J. Tackmann and W. J. Waalewijn, Phys. Rev. Lett. **105**, 092002 (2010).
- [57] D. Krohn, J. Thaler and L. T. Wang, JHEP **0906**, 059 (2009).
- [58] The corresponding code is available from the authors.
- [59] M. Oreglia, SLAC-236 (80,REC.APR. 81), J. Gaiser, SLAC-255 (82,REC.JUN.83) T. Skwarnicki, DESY-F31-86-02.